Environmental Science & Technology

Article

pubs.acs.org/est

Redox Interactions of Tc(VII), U(VI), and Np(V) with Microbially Reduced Biotite and Chlorite

Diana R. Brookshaw,[†] Richard A. D. Pattrick,[†] Pieter Bots,[†] Gareth T. W. Law,[‡] Jonathan R. Lloyd,[†] J. Fredrick W. Mosselmans,[§] David J. Vaughan,[†] Kathy Dardenne,[∥] and Katherine Morris*[,†]

[†]Research Centre for Radwaste Disposal and Williamson Research Centre for Molecular Environmental Science, School of Earth, Atmospheric and Environmental Sciences, The University of Manchester, Oxford Road, Manchester M13 9PL, United Kingdom

[‡]Centre for Radiochemistry Research, School of Chemistry, The University of Manchester, Manchester M13 9PL, United Kingdom

[§]Diamond Light Source Ltd., Diamond House, Harwell Science and Innovation Campus, Didcot, Oxfordshire OX11 0DE, United Kingdom

[∥]Karlsruhe Institute of Technology, Institut fur Nukleare Entsorgung, D-76021 Karlsruhe, Baden-Württemberg, Germany

ABSTRACT: Technetium, uranium, and neptunium are contaminants that cause concern at nuclear facilities due to their long half-life, environmental mobility, and radiotoxicity. Here we investigate the impact of microbial reduction of Fe(III) in biotite and chlorite and the role that this has in enhancing mineral reactivity toward soluble TcO_4^-, UO_2^{2+}, and NpO_2^+. When reacted with unaltered biotite and chlorite, significant sorption of U(VI) occurred in low carbonate (0.2 mM) buffer, while U(VI), Tc(VII), and Np(V) showed low reactivity in high carbonate (30 mM) buffer. On reaction with the microbially reduced minerals, all radionuclides were removed from solution with U(VI) reactivity influenced by carbonate. Analysis by X-ray absorption spectroscopy (XAS) confirmed reductive precipitation to poorly soluble U(IV) in low carbonate conditions and both Tc(VII) and Np(V) in high carbonate buffer were also fully reduced to poorly soluble Tc(IV) and Np(IV) phases. U(VI) reduction was inhibited under high carbonate conditions. Furthermore, EXAFS analysis suggested that in the reaction products, Tc(IV) was associated with Fe, Np(IV) formed nanoparticulate NpO_2, and U(IV) formed nanoparticulate UO_2 in chlorite and was associated with silica in biotite. Overall, microbial reduction of the Fe(III) associated with biotite and chlorite primed the minerals for reductive scavenging of radionuclides: this has clear implications for the fate of radionuclides in the environment.

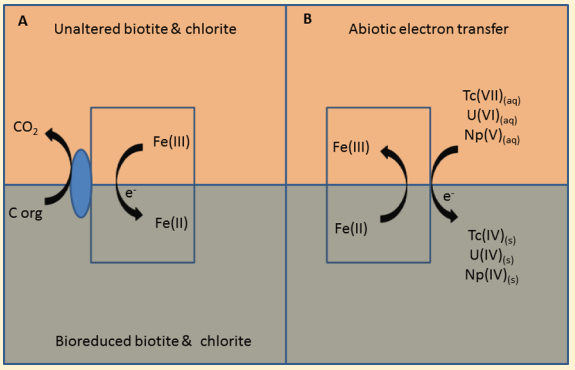

INTRODUCTION

Radionuclide contamination of the subsurface is both significant and problematic at nuclear facilities. Furthermore, in many developed nations, the long-term management strategy for radioactive wastes is disposal in a deep geological disposal facility (GDF). In both contaminated land and deep geological disposal, radionuclide behavior in the geosphere needs to be predicted over extended time scales. This is particularly true for long-lived radionuclides (e.g., ^{99}Tc, U, and ^{237}Np, all with half-lives $>10^5$ years) as they are persistent contaminants at nuclear sites and will make up a significant fraction of the higher activity radioactive waste destined for deep geological disposal.

Microbes are ubiquitous in Earth's shallow subsurface, driving changes in ambient geochemistry; a significant body of work also confirms their presence in the deep subsurface. Indeed, it is becoming clear that they will influence the GDF environment.[1−4] For intermediate level wastes, electron donors used by microbes for anaerobic metabolism will be both present within and generated by the evolving waste-forms, with both cellulose degradation products and hydrogen likely to be significant.[5,6] Reflecting this, microbially mediated reduction in the deep subsurface will be stimulated by radioactive waste disposal, and there is the potential for these processes to impact upon radionuclide behavior in the GDF environment.[1,3,7] Thus, in both the shallow and deep subsurface, a thorough understanding of the biogeochemical interactions of long-lived radionuclides with soil and rock minerals is essential in building a robust safety case for the management of radioactively contaminated land and for the long-term geological disposal of nuclear waste.

In the environment, the mobility of the long-lived radionuclides Tc, U, and Np is governed primarily by their oxidation state with $Tc(VII)O_4^-$, $U(VI)O_2^{2+}$, and $Np(V)O_2^+$, being relatively soluble under oxic conditions and with both sorption and complexation potentially influencing U(VI) and Np(V) mobility.[8] By contrast, reduction of these radionuclides results in

Received: July 21, 2015
Revised: October 20, 2015
Accepted: October 21, 2015
Published: October 21, 2015

DOI: 10.1021/acs.est.5b03463
Environ. Sci. Technol. 2015, 49, 13139−13148

the creation of poorly soluble reaction products with hydrous $Tc(IV)O_2$-like phases as well as Tc^{4+} sorption, $U(IV)O_2$ and monomeric U(IV) species, and Np(IV) phases, respectively, reported in the literature.[3,9−12] Consequently, processes causing reduction of these radionuclides in the environment are expected to retard their mobility. Such reduction may be biotic (direct) due to enzymatic processes or abiotic (indirect chemical reduction), where microbial activity in the subsurface leads to the reduction of e.g. Fe(III) in minerals and the resultant Fe(II) reacts abiotically with the radionuclide. It has been recognized that reduction of Fe(III) leads to the buildup of a store of reactive Fe(II) in sediments generally,[13] and microbially reduced minerals more specifically, including clays and sheet silicates[14−18] although the full impact of these processes on radionuclide solubility has not been fully explored. Briefly, both Tc(VII) and Np(V) are abiotically reduced in the presence of mineral-associated Fe(II).[12,14,17,19−21] The reduction of U(VI) is more complex with direct enzymatic microbial reduction likely to be a dominant process in many systems.[22−26] However, under some abiotic experimental conditions, U(VI) reduction has been observed with pH, Fe(II) speciation, and solution chemistry implicated in controlling the reaction.[27−30]

Two micaceous phyllosilicates, biotite and chlorite, are particularly relevant to radionuclide behavior in the environment as they are abundant in near surface sediments and in many of the crystalline host rocks likely for deep geological disposal. They will probably represent a significant fraction of the reducible Fe(III) in many deep subsurface systems. Interactions of U(VI) with unaltered biotite and chlorite have been the subject of various studies showing that sorption of U(VI) to the minerals is inhibited by carbonate in solution,[31] and abiotic reduction of U(VI) by Fe(II) in the interlayers of "unaltered" biotite is possible over extended reaction times.[32] However, despite the environmental importance of these minerals, the effect of bioreduction on biotite and chlorite and its impact on the speciation and fate of Tc(VII) and U(VI) remains poorly understood, whereas no studies have yet addressed the redox reactivity of these minerals toward Np, a key, long-lived transuranic element in radioactive waste. The objectives of this study were to define radionuclide reactivity and fate with both the unaltered and bioreduced mineral phases and explore the potential for transformation of the oxic, mobile Tc(VII), U(VI), and Np(V) species to reduced, less soluble forms on exposure to bioreduced biotite and chlorite.

MATERIALS AND METHODS

Safety. Technetium-99, uranium, and neptunium-237 are radioactive. Work with radionuclides must be carried out by appropriately qualified and experienced staff at facilities designed for work with radioactive materials. The possession and use of radioactive materials is subject to statutory control.

Microbial Cultures. The Fe(III)-reducing bacterium *Geobacter sulfurreducens* was cultured using aseptic, anaerobic techniques as described previously using a defined medium with acetate as the electron donor and fumarate as the electron acceptor.[16,33] Bacteria used for mineral reduction were harvested at late log phase by centrifugation (5000 *g*, 5 min), before washing twice in anaerobic 30 mM $NaHCO_3$ (pH 7) or 30 mM MOPS (pH 7) with 0.2 mM $NaHCO_3$ for "low carbonate" U(VI) experiments. The harvested and washed cells were resuspended in the respective buffers before addition to minerals and appropriate, experimentally matched cell controls were also prepared.

Mineral Preparation. Minerals were prepared and characterized as described previously,[16,33] and the 180−500 μm biotite (annite-phlogopite) and <100 μm chlorite fractions were used in the experiments. For characterization, the surface area of the unaltered materials was measured by BET analysis, and both total Fe and Fe(III) in the minerals were assessed using electron probe microanalysis (EPMA) and Mössbauer spectroscopy, respectively.[16] Finally, 0.5 N HCl extractable Fe(II)/Fe(III) was measured using ferrozine with and without hydroxylamine hydrochloride reduction and was used as an indicator of changes in the levels of bioavailable Fe in the mineral systems.[34]

Mineral Bioreduction. Microbially reduced minerals were made by stimulating washed cell suspensions of *Geobacter sulfurreducens* to mediate the reduction of Fe(III) in biotite and chlorite via the addition of 10 mM acetate and 0.01 mM of anthraquinone-2,6-disulfonate (AQDS) to act as an electron shuttle.[16,35] The minerals were microbially reduced in batches of 2 g of fresh mineral suspended in 80 mL of 30 mM $NaHCO_3$ at pH 7 under an atmosphere of 80%:20% N_2:CO_2.[16] To initiate microbial reduction, *Geobacter sulfurreducens* was harvested at the late log phase of growth, washed, and then added to the mineral slurry to a final OD_{600} of ∼0.2. At this stage, the microbially reduced minerals and biomass were separated from the aqueous phase by centrifugation at 4 °C (5000 *g*, 5 min) and then washed twice to remove any residual electron donor with anaerobic deionized water under an anaerobic atmosphere. The microbially reduced minerals were then stored as a 1:5 slurry in anaerobic, deionized water at 4 °C until use, typically within 4 weeks of preparation.

Radionuclide Reduction Experiments. Biotite or chlorite, either in their fresh or microbially reduced form, were used in a solid:solution ratio of 1:100 in anaerobic batch experiments, with a solution of 30 mM $NaHCO_3$ under an 80:20% N_2:CO_2 atmosphere at pH 7. For the low carbonate U(VI) experiments, 30 mM MOPS buffer at pH 7 with 0.2 mM $NaHCO_3$ under an N_2 atmosphere was used. In addition, controls with buffer solutions only and cell only controls (no electron donor) were included. For the latter, cells from the same batch as were used for the mineral preparation were added to the buffer to a final OD_{600} ∼ 0.2. All experiments were run in triplicate.

The batch experiments were left to equilibrate for 24 h with the mineral and then spiked with $^{99}Tc(VII)$ from a 0.1 M ^{99}Tc stock, U(VI) from a 10 mM U(VI) in 0.001 M HCl stock, or $^{237}Np(V)$ from an ∼0.01 M Np(V) stock prepared according to the method of Law et al.,[12] to allow reaction. The U(VI) experiments were run at a final concentration of 0.126×10^{-3} M U(VI). The removal of Tc and Np from solution was tracked in low-level experiments, where Tc(VII) was spiked to give a final concentration of 1.6×10^{-6} M (100 Bq ml^{-1}) and Np (V) at 1.6×10^{-6} M (10 Bq mL^{-1}). Parallel, higher activity experiments were run for Tc(VII) and Np(V) (∼0.2×10^{-3} M and ∼0.1×10^{-3} M, respectively) to generate solid samples at several hundred ppm for XAS analysis.

After spiking, the concentrations of the radionuclides in the supernatant were determined periodically on centrifuged samples (5000 *g*, 5 min). For aqueous U(VI), aliquots were analyzed by colorimetric assay.[36] The total concentration of Tc in solution was analyzed by liquid scintillation counting (Tri-Carb 2100 TR Scintillation Counter, Packard; Optiphase HiSafe 3 Liquid Scintillant, PerkinElmer; detection limit of ∼0.5 Bq per 1 mL sample). The total concentration of Np in solution was analyzed by ICP-MS using an Agilent 7500cx (in 2% HNO_3) with ^{232}Th added as an internal standard.

DOI: 10.1021/acs.est.5b03463
Environ. Sci. Technol. 2015, 49, 13139−13148

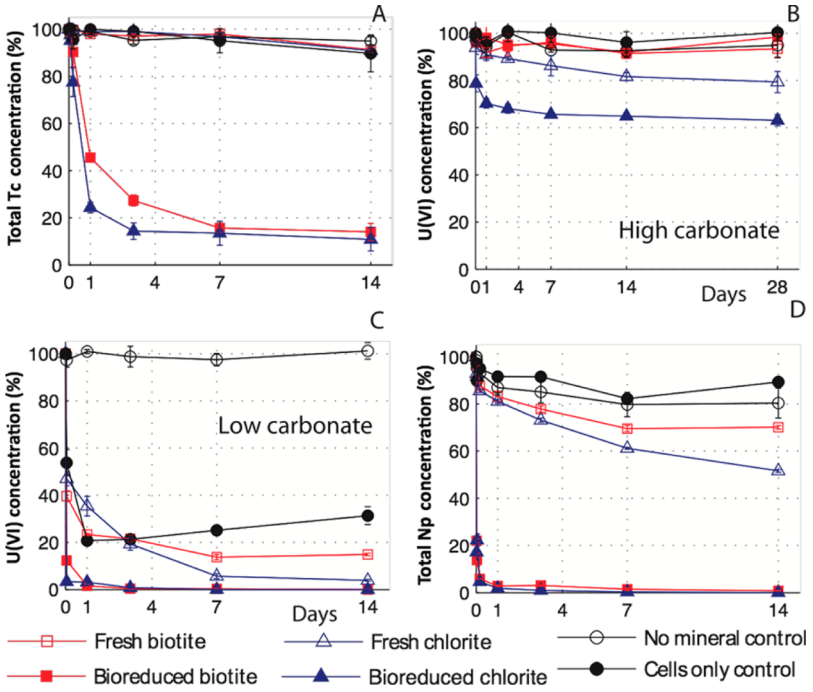

Figure 1. Concentrations of U, Tc, and Np in solution with time after reaction with biotite and chlorite. (A) Tc(VII) reaction with unaltered and bioreduced biotite and chlorite (1:100, pH 7, 30 mM HCO_3^-); (B) U(VI) reaction with unaltered and bioreduced biotite and chlorite (1:100, pH 7, 30 mM HCO_3^-); (C) U(VI) reaction with unaltered and bioreduced biotite and chlorite (1:100, pH 7, 0.2 mM HCO_3^-, 30 mM MOPS buffer); (D) Np(V) reaction with unaltered and bioreduced biotite and chlorite (1:100, pH 7, 30 mM HCO_3^-). Error bars represent 1σ standard deviation of the mean of triplicate measurements. Appropriate media only (no mineral), and cell only (no electron donor) controls are also shown.

XAS Analysis. Samples for X-ray absorption spectroscopy (XAS) analysis were obtained at the end point of each experiment from Tc(VII) reacted with microbially reduced biotite and chlorite; U(VI) reacted with both unaltered and microbially reduced biotite and chlorite in low carbonate buffer; U(VI) reacted with microbially reduced chlorite in high carbonate buffer; and Np(V) reacted with microbially reduced biotite and chlorite. All sample manipulations were performed under anaerobic conditions, and the mineral residues were separated by centrifugation (5000 *g*, 5 min) prior to mounting in airtight, approved sample cells and storage at −80 °C under argon until analysis. In-house U(VI) (schoepite) and U(IV) (biogenic uraninite) standards were analyzed, and additional Tc(IV) (TcO_2), Tc(VII) (TcO_4^-), Np(IV) (Np^{4+}), and Np(V) (NpO_2^+) standards were obtained from the relevant literature.[37−39]

The X-ray absorption spectroscopy (XAS) analyses of Tc K-edge and U-L_{III} edge samples were performed at beamline B18 at Diamond Light Source Ltd., UK using a Si (111) double crystal monochromator. The spectra were collected in fluorescence mode at room temperature, with a 9-element solid-state Ge detector system.[40] Spectra for the U(VI) and U(IV) standards were collected in transmission mode. Neptunium L_{III} edge XAS analyses were performed at the INE Beamline for actinide research at the ANKA Light Source (Germany) in fluorescence mode using a 5-element solid state Ge detector with a Ge (422) monochromator crystal.[41] Energy calibration for the XAS analyses of Tc, U, and Np was performed using molybdenum, yttrium, and zirconium foils. XAS data reduction, energy calibration, and fitting were performed using the Demeter software package,[42] and FEFF8 was used to calculate the scattering paths.[43]

RESULTS AND DISCUSSION

Mineral Characterization. The biotite and chlorite used in these experiments have previously been extensively characterized.[16,44] The unaltered minerals had a similar surface area measured by BET of 9.0 $m^2\ g^{-1}$ and 6.4 $m^2\ g^{-1}$, respectively, and contained 17.1 ± 0.1 wt % and 38.4 ± 0.1 wt % total iron. Of that iron, 0.5 N HCl acid-extractable iron was measured as 71 ± 1% Fe(II) and 56 ± 1% Fe(II), respectively. Microbially mediated Fe(III) reduction led to an increase in acid-extractable Fe(II) to 96 ± 1% of Fe(II) in biotite and 85 ± 2% Fe(II) in chlorite. This represented a significant transformation of Fe(III) to Fe(II) in the minerals of ∼0.16 mmol g^{-1} in biotite and ∼0.15 mmol g^{-1} in chlorite.[16] In comparison, recent work on bioreduction of the phyllosilicate nontronite suggested a higher bioreduction potential with ∼1.5 mmol g^{-1} of Fe(II) reported after two bioreduction cycles.[18] In parallel, non-active experiments with the same minerals and under the same conditions of the current study, bioreduction of the 0.5 N HCl acid extractable Fe(III) in biotite was essentially complete after 3 days (24 h with the electron shuttle, AQDS) and reached 90% for chlorite after 3 days.[16] The reduced Fe(II) was retained as sorbed Fe or at edge/internal sites on the mineral with only minor release of Fe to solution during reduction confirming the reduction process was a predominantly solid state reaction. On bioreduction, no structural changes or new phases were detected by X-ray diffraction, although 0.5 N HCl acid leaching experiments showed bioreduced samples were more susceptible to dissolution of Si, Mg, and Fe compared to untreated samples suggesting reduced mineral stability post-reduction. Imaging of bacterial cells showed a preference for initial cell growth at biotite steps on the mineral 001 surface (where the tetrahedral sheet is accessible) followed by colony growth over the surface.[44] Overall, the bioreduced, reactive iron was the key phase that

DOI: 10.1021/acs.est.5b03463
Environ. Sci. Technol. 2015, 49, 13139−13148

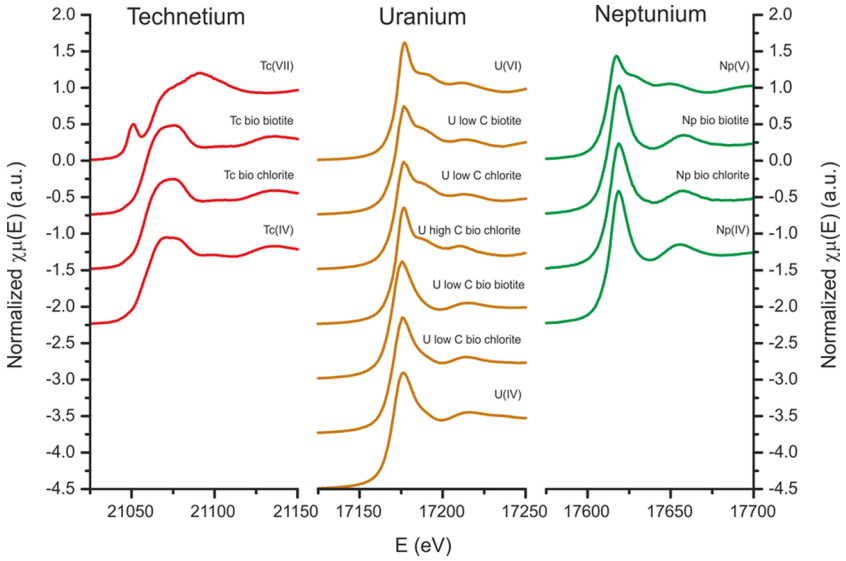

Figure 2. Normalized Tc K-edge and U and Np L_{III}-edge XANES spectra of the unaltered and bioreduced biotite and chlorite Tc, U, and Np samples. The plot includes relevant reference spectra including Tc(IV) and Tc(VII) standards, in-house U(IV) and U(VI) standards, and Np(IV) and Np(V) standards.[37−39]

was able to facilitate Cr(VI) reduction to Cr(III) in experiments similar to those discussed here.[16]

Radionuclide Removal in Experiments. Both Tc(VII) and U(VI) were fully soluble (5000 *g*, 5 min) in the no mineral control buffer solutions, while Np(V) showed modest removal from the 30 mM buffer with 80.4 ± 6.4% of Np(V) soluble in the buffer at 14 days (Figure 1). This was despite the fact that PHREEQC modeling with both the SIT and LLNL databases predicted under saturation of Np(V) in the buffer solution at ~10^{-6} M Np(V). Similarly, in the cells only controls with no electron donor, Tc(VII) and U(VI) in the high carbonate system were, within error, fully retained in solution over the experimental time course, and Np(V) again showed only ~20% removal suggesting the cells alone did not provide any significant sorption or reduction capacity in these systems (Figure 1). Interestingly, for U(VI) the low carbonate, cells only controls with no electron donor did show significant U removal (~70%). The XANES analysis for this sample confirmed the U was speciated as U(VI) (Figure 2), and thus the removal was due to sorption of U(VI) to biomass again confirming no significant reduction capacity was retained in the electron donor free cell controls.

On reaction with minerals, the Tc(VII) system showed no removal by the unaltered minerals, while in the microbially reduced experiments, extensive Tc removal occurred (86.0 ± 3.6% by biotite and 89.1 ± 8.9% by chlorite) by the experimental end point (Figure 1 A). For U(VI) in the high carbonate buffer with unaltered minerals, there was no removal with biotite and only modest removal with chlorite (20 ± 3%). This was similar to previously published data on 30 mM carbonate systems showing scant removal of U(VI) by unaltered chlorite over time scales of days.[25] The U experiments with microbially reduced minerals in high carbonate buffer showed essentially no removal of U(VI) with biotite, while chlorite was slightly more reactive after microbial reduction with 37 ± 2% U sorbed to the solid phase after 14 days (Figure 1 B). For U(VI) the experiment was run at relatively high (0.126 mM U(VI)) concentrations compared to Tc and Np systems (which were at ~1 μM concentrations). Even so, in terms of electron balance, there was a greater than 6-fold stoichiometric excess of mineral-associated, biogenic and thus reactive Fe(II) (~0.15 m mol per 100 mL experiment[16]) compared to U(VI) (0.012 m mol per 100 mL experiment); the system reactivity was therefore not limited by reactive Fe(II) in the microbially reduced mineral experiments. For the low carbonate system, both the unaltered and microbially reduced minerals showed significant reactivity toward U(VI) with >80% removal in all systems, although it is clear that the microbially reduced phases showed the highest reactivity with essentially complete removal at 14 days (Figure 1C). The different behavior of U(VI) in the low and high carbonate systems is related to the influence of carbonate on the system as uranyl-carbonates are known to decrease U(VI) adsorption to mineral surfaces, lower the U(VI)/U(IV) redox couple, and retard the kinetics of U(VI)-reduction.[45,46] Indeed, recent work has highlighted the importance of aqueous, noncarbonate UO_2^{2+} as the most readily reducible aqueous uranyl species.[47] These factors support the observations in our experiments that U(VI) reactivity is enhanced in the low carbonate systems compared to the high carbonate systems. Finally, the Np(V) reaction with unaltered biotite and chlorite showed slightly increased removal compared to the groundwater and cell only controls with 30.1 ± 0.7% and 48.4 ± 0.6% removal at the experiment end points. For both of the microbially reduced minerals, and in contrast to the parallel U(VI) experiment in high carbonate buffer, Np(V) was quickly scavenged to below the detection limit (<4×10^{-11} M) within 24 h (Figure 1D). Overall, the microbially reduced mineral phases showed enhanced reactivity to Tc(VII), U(VI) in low carbonate, and Np(V) with relatively poor reactivity in the U(VI) high carbonate system, the latter presumably as a result of the influence of carbonate on U(VI)-reactivity.

Radionuclide Speciation. In order to characterize the speciation of the radionuclides on reaction with the minerals, selected samples were analyzed using X-ray absorption spectroscopy. Throughout, where possible both XANES and EXAFS spectra were analyzed in order to assess the oxidation state and coordination environment of the radionuclides in these complex samples. For Tc, the K-edge positions for the XANES spectra for microbially reduced biotite and chlorite matched the Tc(IV)

DOI: 10.1021/acs.est.5b03463
Environ. Sci. Technol. 2015, 49, 13139−13148

Table 1. Details of the EXAFS Fit Parameters for the Tc K-Edge and U and Np L_{III}-Edge EXAFS of the Unaltered and Bioreduced Biotite and Chlorite Samples[a]

	scattering path	*N*	*R*	σ^2	$S0^2$	R-factor
Tc bioreduced chlorite	Tc−O	6*	2.01	0.004(1)	0.8*	0.016
	Tc−Tc	1.5 (7)	2.51	0.007(3)		
	Tc−O−Tc−O	6*	4.02*	0.008*		
Tc bioreduced chlorite + 1 Fe	Tc−O	6*	2.00(1)	0.005(1)	0.8*	0.007
	Tc−Tc	1.6(4)	2.51(1)	0.004(2)		
	Tc−Fe	1*	2.57*	0.006(5)		
	Tc−O−Tc−O	6*	4.01*	0.010*		
Tc bioreduced chlorite + 0.5 Fe	Tc−O	6*	2.00(1)	0.004(1)	0.8*	0.008
	Tc−Tc	1.2(5)	2.52(2)	0.003(4)		
	Tc−Fe	0.5*	2.57*	0.003(10)		
	Tc−O−Tc−O	6*	3.96*	0.009*		
Tc bioreduced biotite	Tc−O	6*	2.00(1)	0.004(1)	0.8*	0.017
	Tc−Tc	1.4 (8)	2.50(2)	0.009(5)		
	Tc−O−Tc−O	6*	4.00*	0.008*		
Tc bioreduced biotite + 1 Fe	Tc−O	6*	1.99(1)	0.004(1)	0.8*	0.007
	Tc−Tc	1.3(4)	2.53(1)	0.003(2)		
	Tc−Fe	1*	2.57*	0.005(5)		
	Tc−O−Tc−O	6*	3.98*	0.009*		
Tc bioreduced biotite + 0.5 Fe	Tc−O	6*	2.00(1)	0.004(1)	0.8*	0.009
	Tc−Tc	1.0(3)	2.52(3)	0.003(4)		
	Tc−Fe	0.5*	2.57*	0.002(10)		
	Tc−O−Tc−O	6*	3.99*	0.009*		
U low carbonate unaltered biotite	$U-O_{ax}$	2*	1.79(1)	0.001(2)	1.0*	0.015
	$U-O_{eq\ 1}$	3*	2.31(2)	0.002(1)		
	$U-O_{eq\ 2}$	3*	2.50(2)	0.004*		
	$U-O_{ax}-O_{ax}$	2*	3.59*	0.003*		
	$U-O_{ax}-U-O_{ax}$	2*	3.59*	0.003*		
	$U-O_{ax}-U-O_{ax}$	2*	3.59*	0.007*		
U low carbonate unaltered chlorite	$U-O_{ax}$	2*	1.79(1)	0.002(1)	1*	0.015
	$U-O_{eq}$	5*	2.36(2)	0.015(2)		
	$U-O_{ax}-O_{ax}$	2*	3.58*	0.005*		
	$U-O_{ax}-U-O_{ax}$	2*	3.58*	0.005*		
	$U-O_{ax}-U-O_{ax}$	2*	3.58*	0.009*		
U low carbonate bioreduced biotite	U−O	5*	2.33(3)	0.009(4)	0.7(2)	0.025
	U−O	2*	2.52(9)	0.009*		
	U−Si	2*	3.20(5)	0.012(7)		
U low carbonate bioreduced chlorite	U−O	3*	2.22(2)	0.005(2)	1*	0.041
	U−O	4*	2.39(2)	0.006(2)		
	U−U	5*	3.83(3)	0.011(2)		
U high carbonate bioreduced chlorite	$U-O_{ax}$	2*	1.80(1)	0.003(1)	1*	0.0123
	$U-O_{eq}$	6*	2.45(1)	0.009(1)		
	U−C	3*	2.91(1)	0.003(1)		
	$U-O_{ax}-O_{ax}$	3*	3.60*	0.006*		
	$U-O_{ax}-U-O_{ax}$	2*	3.60*	0.006*		
	$U-O_{ax}-U-O_{ax}$	2*	3.60*	0.013*		
	$U-O_{dist}$	3*	4.20(2)	0.004(3)		
	$U-C-O_{dist}$	6*	4.20*	0.007*		
	$U-C-O-C_{dist}$	3*	4.20*	0.010*		
Np bioreduced biotite	Np−O	8*	2.34(2)	0.009(2)	1.0(2)	0.036
	Np−O−O	24*	3.69*	0.019*		
	Np−Np	4*	3.82(3)	0.007(3)		
Np bioreduced chlorite	Np−O	8*	2.34(2)	0.009(2)	1.0(2)	0.031
	Np−O−O	24*	3.69*	0.018*		
	Np−Np	4*	3.81(3)	0.008(3)		

[a] *N*, *R*, σ^2, $S0^2$, and the R-factor refer to the coordination number, radial distance, Debye−Waller factor, amplitude correction factor, and the goodness of fit, respectively. The asterisks denote that these variables were fixed or linked to previous shells. Throughout, for the Tc, U, and Np samples respectively, the value of $S0^2$ was refined using known coordination numbers (e.g., for Tc−O the coordination number was 6) for each edge and then fixed to the mean value obtained in Artemis fitting. This approach was successful for the Tc, Np, and all but one of the U samples, the U low carbonate bioreduced biotite sample. For this data set leaving $S0^2$ fixed at or even near to 1 would not give a good, chemically credible fit. Thus,

DOI: 10.1021/acs.est.5b03463
Environ. Sci. Technol. 2015, 49, 13139−13148

Table 1. continued

$S0^2$ was refined to a value 0.70. As the coordination numbers and Debye−Waller factors for this fit are reasonable, it suggests that during data collection a reduction of the EXAFS amplitude occurred. The cause is uncertain but may have been detector nonlinearity or sample inhomogeneity.

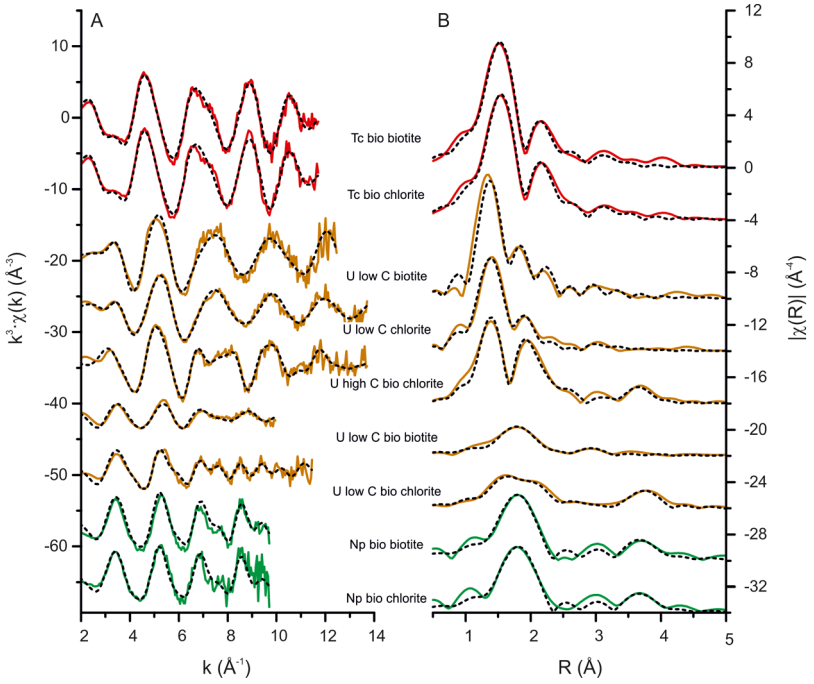

Figure 3. Technetium K-edge, uranium L_{III}-edge, and neptunium L_{III}-edge EXAFS spectra for Tc(VII) reacted with bioreduced biotite and magnetite; U(VI) reacted with unaltered minerals in low carbonate (0.2 mM) medium, with bioreduced chlorite in high carbonate (30 mM) medium, and with bioreduced biotite and chlorite in low carbonate (0.2 mM) medium; and Np(V) reacted with bioreduced biotite and chlorite. Panel A k^3-weighted EXAFS; panel B − Fourier transform of k^3-weighted EXAFS, "bio" is used to indicate bioreduced mineral systems. Dashed lines show experimental data, and colored lines show the best fits described in Table 1.

reference (Figure 2).[37] There was no evidence of the distinct Tc(VII) pre-edge peak at 21045−21050 eV confirming essentially complete reduction to Tc(IV) (Figure 2). Interestingly, there was no double peak in the absorption edge of the spectra, which has previously been attributed to octahedrally coordinated Tc and/or Tc−Fe interactions.[48,49] Overall, the Tc XANES spectra show that little Tc(VII) is present on microbially reduced biotite and chlorite (Figure 2). The Tc K-edge EXAFS of the two samples were very similar. Initially both spectra were fitted with a hydrous TcO_2-like model[9] with the best fit including 6 O at 2.00 Å and ∼1.5 Tc at 2.51 Å, suggesting a chain length of ∼3 edge sharing Tc polyhedra (see Table 1; Figure 3). The EXAFS for both samples had features that were not fully resolved with this model alone, and further consideration of additional shells of backscatterers informed by the relevant literature[17,50,51] provided improvements to the initial fitting for each sample (Table 1). A fit with ∼1.5 Tc at 2.52 Å and one additional "short" Fe backscatterer at ∼2.57 Å improved the fit (Table 1). This type of short Tc−Fe interaction has been attributed previously to Tc(IV) interactions with Fe-bearing solids and where both short polymeric TcO_2 chain lengths and attachment to surface Fe−O octahedra have been implicated.[48,50−53] The Tc EXAFS for both biotite and chlorite resemble data dealing with Tc-nontronite interactions[17] where short chain hydrous TcO_2 without an Fe-interaction was observed, and data for Tc(IV) interactions with both sediments and magnetite[51,53] where short chain hydrous TcO_2-Fe interactions were modeled. In our systems, inclusion of 1 Fe at 2.57 Å showed improvement to the fit, while a fit with 0.5 Fe at 2.57 Å, perhaps a more realistic fit for the Fe contribution in a short polymeric TcO_2 chain tethered to Fe O octahedra, also improved the fit but to a lesser extent (Table 1). Interestingly, a fit with Si backscatterers was possible in both samples, but consideration of the ionic radii for Si (0.4 Å) versus Fe (0.79 Å) meant that the fitting distance for Si of ∼2.86 Å seemed unduly long compared to the "short Fe" fit while fitting with a closer Si backscattering shell was unsatisfactory. This is in agreement with recent work on Tc reactivity in hyperalkaline systems where aluminosilicate dissolution had occurred which suggested physical overcoating of Tc by aluminosilicates rather than chemical bonding was controlling Tc(IV) behavior.[54] Overall for Tc, the additional Fe backscatterer interactions we modeled provided an improved fit in the EXAFS modeling suggesting associations between the hydrous TcO_2 product and Fe within the microbially altered mineral systems.

In the U(VI) high carbonate system, XAS analysis was possible only for the microbially reduced chlorite system which showed ∼37% removal of U(VI) to solids over 2 weeks (Figure 1B). Here, the U L_{III}-edge XANES edge position and spectrum were essentially the same as the U(VI) standard, and there was no evidence for significant U(VI)-reduction over the experimental duration (Figure 2). The corresponding EXAFS for this sample could be modeled using a U(VI) triscarbanato model,[55,56] which suggested outer sphere complexation of a U(VI)-carbonate anion to the chlorite similar to the observations of Zhang et al.[25] (Table 1, Figure 3). For U(VI) experiments in the low carbonate systems, U L_{III}-edge XAS spectra were collected from the unaltered and microbially reduced minerals. In the unaltered mineral experiments, the U XANES edge positions for both

DOI: 10.1021/acs.est.5b03463
Environ. Sci. Technol. 2015, 49, 13139−13148

samples were aligned with the U(VI) standard, and there was no evidence for significant U(VI)-reduction over the experimental duration (Figure 2). Interestingly, different sorption and reduction behavior of U(VI) with unaltered biotite and chlorite has been observed in the literature. For example, U(VI)-chlorite experiments in carbonate media showed U(VI) sorption but little reduction,[25,31] while U(VI)-biotite experiments in the absence of carbonate showed reduction to U(IV).[29] In our systems, which had modest levels of carbonate (0.2 mM), after 2 weeks there was no evidence for significant reduction of U(VI) in the XAS data confirming that sorption of U(VI) was dominant in these low carbonate experiments. By contrast, for the low carbonate U(VI) experiments with microbially reduced biotite and chlorite, there was a marked change in the XANES spectra with the edge position for both samples similar to that of the U(IV) standard, and the spectra themselves showing similar features to U(IV), notably with an absence of any uranyl multiple scattering features (Figure 2). These data confirm that in the low carbonate systems, the microbially reduced minerals enhanced the removal of U(VI) from solution via reductive transformation to poorly soluble U(IV). The U L_{III} edge EXAFS of experiments with the unaltered minerals in low carbonate were fitted with a typical U(VI) coordination environment with, for biotite, 2 O at 1.80 Å and a split shell of 3 O at 2.32 Å and 3 O at 2.51 Å and for chlorite 2 O at 1.79 Å and 6 O at 2.33 Å, and with no clear benefit in adding additional shells to the fit (Table 1, Figure 3). By contrast, the EXAFS spectra for the U reaction products on the microbially reduced minerals in low carbonate experiments were clearly different both to the unreacted controls and also differed between the biotite and chlorite systems. For chlorite, a best fit U(IV) model had a split shell of 3 O at 2.22 Å and 4 O at 2.39 Å, consistent with a U(IV) coordination environment. Again, it was clear the EXAFS spectrum for this sample had features that were not fully resolved with this model alone, and consideration of the relevant literature on U(IV)-chlorite interactions[31] allowed us to confidently fit an additional contribution of U backscatterers (5 U at 3.83 Å). This fit strongly supported uranium in a uraninite-like coordination environment in the bioreduced chlorite (Table 1, Figure 3). The reduced occupancy of U in the backscattering shell at 3.83 Å, in this case fitted with 5 U backscatterers, compared to crystalline UO_2 (12 U at ∼3.85 Å[57]) is consistent with the formation of nanoparticulate UO_2 (e.g. ref 58) as observed in abiotic U-chlorite experimental systems.[31] The microbially reduced biotite product could best be modeled with a U(IV)-like coordination environment with a split shell of 5 O at 2.33 Å and 2 O at 2.52 Å consistent with a U(IV) coordination environment. Again, additional features were present in the EXAFS spectrum which were not fully resolved in the fit, and several likely additional backscatterers including U, C, and P[58−60] were considered in additional fits. Here, the additional contribution was best modeled with 2 Si backscatterers at ∼3.2 Å, and notably, fits for monomeric C and P backscatterers informed by the relevant literature[59,60] were poor when compared to the fit for Si as a backscatterer (Table 1, Figure 3). Indeed, it is notable that the U−Si bond fitted at 3.2 Å in our study is consistent with the short U−Si bond observed in coffinite.[61] A similar fit has recently been observed in U(IV)-silicate colloid systems[62] where it was postulated that silicate was bonding with U(IV) and also that there was significant structural disorder in the U(IV)-silicate product with no evidence for U−U backscatterers. Interestingly, past work has identified that U(VI) reduction can occur at both edge sites and interlayer sites within biotite[32] suggesting the potential for a structured binding environment for U(IV), and our data suggest there is some evidence for a direct U(IV)-silicate interaction. Overall, the U data showed U(VI) sorption to biotite and chlorite in the unaltered mineral systems with carbonate influencing the speciation of the sorption product. For microbially reduced biotite and chlorite, in the high carbonate chlorite experiment, sorption but no reduction occurred, and outer sphere complexation of U(VI)-triscarbanato species was modeled. In low carbonate experiments, U(IV) species dominated, and intriguingly there was evidence that a U(IV)-silicate interaction occurred in the biotite system.

Finally, for neptunium, the Np L_{III}-edge XANES spectra of the microbially reduced mineral samples resembled the spectrum of the Np(IV) standard confirming reduction to Np(IV) in both mineral systems. The EXAFS of the biotite and chlorite samples were very similar and were both fitted by a Np(IV)O_2 model with 8 O backscatterers at a Np−O distance of 2.34 Å and with the fit for both minerals significantly improved by the addition of 4 Np backscatterers at 3.82 Å. This is comparable to the published EXAFS data for crystalline NpO_2[63] but again, and parallel to the U(IV)-chlorite system, with reduced occupancy compared to the crystalline phase (4 Np in the current study rather than 12 Np in the crystalline NpO_2, Table 1).[63] In addition, the Debye−Waller factors (σ^2) for our fit were much higher than the published σ^2 values for crystalline NpO_2 (for the Np−Np backscattering interaction at 3.81 Å, values were 0.008 in our study (Table 1) and 0.002[63]), and this suggests a nanoparticulate and disordered solid product. Overall for Np the EXAFS suggest a common nanoparticulate NpO_2 reaction product in both the microbially reduced biotite and chlorite systems similar to recent work where nanoparticulate NpO_2 was precipitated from carbonate solutions.[63] This is in contrast to environmental reduction products observed in more complex mineral/sediment systems where an absence of a Np−Np backscatterer was noted in work on reactions of Np(V) with clays[64] and where Np interactions with Fe-oxides have been discussed[12] and suggests complex controls on the fate of Np(IV) in environmental media.

RELEVANCE TO THE NUCLEAR LEGACY

These results provide clear evidence that the interactions between bacteria and minerals in the subsurface can have a major effect on radionuclide mobility. For biotite and chlorite, it is clear that reactivity toward contaminants is associated with redox cycling the small fraction of Fe in the minerals, the reactive Fe(III), that is susceptible to biotransformation.[16,44] Here we extend this observation to Tc(VII), U(VI), and Np(V), all important long-lived radionuclides in radioactive wastes. When the reactive Fe(III) fraction remained oxidized in the unaltered minerals, there was no significant reduction of U(VI), Tc(VII), and Np(V), and removal from solution was governed by the extent of sorption of the oxidized radionuclides under the prevailing geochemical conditions. Upon microbial reduction, the reactive Fe(III) in the minerals is transformed to reactive Fe(II) at both surface and edge sites[16] similar to recent work on nontronite;[18] this dramatically increases the reducing capacity of the minerals. This change in redox reactivity results in reduction of Tc(VII) and Np(V), removing both from solution readily in high carbonate media. For Tc, analysis of the EXAFS spectra for the reaction products suggest not only that a hydrous TcO_2-like phase forms after interaction with the microbially reduced minerals but also that interactions with Fe occur. For Np, the EXAFS analyses suggest that nanoparticulate NpO_2-like phases form on exposure to the bioreduced mineral similar to those

DOI: 10.1021/acs.est.5b03463
Environ. Sci. Technol. 2015, 49, 13139−13148

discussed in a recent study[63] and in contrast to earlier sediment microcosm and clay studies with this radionuclide.[12,64] For U, reduction to U(IV) only occurred in the microbially reduced treatments and then only in the low carbonate experiments. Here, the U(IV) reaction products differed depending on the mineral system with EXAFS analysis suggesting a U(IV)-silicate interaction in the biotite experiment and a nanoparticulate UO_2 phase in the chlorite system. The detailed mechanisms for U reaction with Si in biotite are as yet unclear, but recent work suggests that electron transfer can occur across tetrahedral sheets in the mineral system suggesting silica rich surfaces may be points of electron transfer in the mineral.[65] Overall, microbially reduced phyllosilicates have the potential to be particularly important in controlling radionuclide behavior in granitic rocks where they represent the main redox active components. In altered mafic igneous rocks the chlorite content will be significant as it will be in mature iron-bearing mudstones. This work shows that it may be possible to prime both these lithologies, and anaerobic phyllosilicate-bearing soils, by stimulating microbial activity for indirect reductive removal of radionuclides as has been observed in past shallow subsurface systems.[13] Furthermore, the presence of elevated carbonate in some regional groundwaters has important implications for abiotic reduction of U(VI) and thus for U-mobility in candidate lithologies surrounding a GDF. The complexity of the reaction products across the different experimental systems is also noteworthy, and it is clear that the long-term stability and evolution of these radionuclide-mineral interaction products warrants continuing investigation to inform planning for nuclear decommissioning and waste management.

AUTHOR INFORMATION

Corresponding Author

*Phone: 44 161 2757541. E-mail: katherine.morris@manchester.ac.uk.

Notes

The authors declare no competing financial interest.

ACKNOWLEDGMENTS

This work was funded through the EPSRC BANDD consortium (EP/G063699/1) and the NERC BIGRAD consortium (NE/H007768/1). Diamond Light Source is thanked for providing Beamtime grants SP7367 and SP7593, the ANKA INE Beamline for access via Actinet, and Env-Rad-Net for support to Morris and Law for data analysis whilst at ANKA INE Beamline. We thank Dr. Steve Parry, Richard Doull, and Dr. Tim Marshall for assistance in sample handling and data collection at Diamond, Paul Lythgoe for ICP-MS analysis and Katie Law for radiochemistry assistance.

REFERENCES

(1) Rizoulis, A.; Steele, H. M.; Morris, K.; Lloyd, J. R. The potential impact of anaerobic microbial metabolism during the geological disposal of intermediate-level waste. *Mineral. Mag.* **2012**, *76* (8), 3261−3270.

(2) Williamson, A. J.; Morris, K.; Shaw, S.; Byrne, J. M.; Boothman, C.; Lloyd, J. R. Microbial reduction of Fe(III) under alkaline conditions relevant to geological disposal. *Appl. Environ. Microbiol.* **2013**, *79* (11), 3320−3326.

(3) Behrends, T.; Krawczyk-Bärsch, E.; Arnold, T. Implementation of microbial processes in the performance assessment of spent nuclear fuel repositories. *Appl. Geochem.* **2012**, *27* (2), 453−462.

(4) Wouters, K.; Moors, H.; Boven, P.; Leys, N. Evidence and characteristics of a diverse and metabolically active microbial community in deep subsurface clay borehole water. *FEMS Microbiol. Ecol.* **2013**, *86* (3), 458−473.

(5) Bassil, N. M.; Bryan, N.; Lloyd, J. R. Microbial degradation of isosaccharinic acid at high pH. *ISME J.* **2015**, *9* (2), 310−320.

(6) Rizoulis, A.; Milodowski, A. E.; Morris, K.; Lloyd, J. R. Bacterial diversity in the hyperalkaline Allas Springs (Cyprus), a natural analogue for a cementitious radioactive waste repository. *Geomicrobiol. J.* **2015**, 00.

(7) Williamson, A. J.; Morris, K.; Law, G. T. W.; Rizoulis, A. R.; Charnock, J. M.; Lloyd, J. R. Microbial reduction of U(VI) under alkaline conditions: Implications for radioactive waste geodisposal. *Environ. Sci. Technol.* **2014**, *48*, 13549−13556.

(8) Dozol, M.; Hagemann, R.; et al. Radionuclide migration in groundwater: a review of the behaviour of actinides. *Pure Appl. Chem.* **1993**, *65*, 1081−1102.

(9) Lukens, W. W.; Bucher, J. J.; Edelstein, N. M.; Shuh, D. K. Products of pertechnetate radiolysis in highly alkaline solution: Structure of $TcO_2 \bullet xH_2O$. *Environ. Sci. Technol.* **2002**, *36* (5), 1124−1129.

(10) Bargar, J. R.; Reitmeyer, R.; Lenhart, J. J.; Davis, J. A. Characterization of U(VI)-carbonato ternary complexes on hematite: EXAFS and electrophoretic mobility measurements. *Geochim. Cosmochim. Acta* **2000**, *64* (16), 2737−2749.

(11) Lear, G.; McBeth, J. M.; Boothman, C.; Gunning, D. J.; Ellis, B. L.; Lawson, R. S.; Morris, K.; Burke, I. T.; Bryan, N. D.; Brown, A. P.; Livens, F. R.; Lloyd, J. R. Probing the biogeochemical behavior of technetium using a novel nuclear imaging approach. *Environ. Sci. Technol.* **2010**, *44* (1), 156−162.

(12) Law, G. T. W.; Geissler, A.; Lloyd, J. R.; Livens, F. R.; Boothman, C.; Begg, J. D. C.; Denecke, M. A.; Rothe, J.; Dardenne, K.; Burke, I. T.; Charnock, J. M.; Morris, K. Geomicrobiological redox cycling of the transuranic element neptunium. *Environ. Sci. Technol.* **2010**, *44* (23), 8924−8929.

(13) Fredrickson, J. K.; Zachara, J. M.; Kennedy, D. W.; Kukkadapu, R. K.; McKinley, J. P.; Heald, S. M.; Liu, C.; Plymale, A. E. Reduction of TcO_4^- by sediment-associated biogenic Fe(II). *Geochim. Cosmochim. Acta* **2004**, *68* (15), 3171−3187.

(14) Bishop, M. E.; Dong, H. L.; Kukkadapu, R. K.; Liu, C. X.; Edelmann, R. E. Bioreduction of Fe-bearing clay minerals and their reactivity toward pertechnetate (Tc-99). *Geochim. Cosmochim. Acta* **2011**, *75* (18), 5229−5246.

(15) Bishop, M. E.; Glasser, P.; Dong, H.; Arey, B.; Kovarik, L. Reduction and immobilization of hexavalent chromium by microbially reduced Fe-bearing clay minerals. *Geochim. Cosmochim. Acta* **2014**, *133*, 186−203.

(16) Brookshaw, D. R.; Coker, V.; Lloyd, J.; Vaughan, D.; Pattrick, R. Redox interactions between Cr(VI) and Fe(II) in bioreduced biotite and chlorite. *Environ. Sci. Technol.* **2014**, *48* (19), 11337−11342.

(17) Jaisi, D. P.; Dong, H.; Plymale, A. E.; Fredrickson, J. K.; Zachara, J. M.; Heald, S.; Liu, C. Reduction and long-term immobilization of technetium by Fe(II) associated with clay mineral nontronite. *Chem. Geol.* **2009**, *264* (1−4), 127−138.

(18) Zhao, L.; Dong, H.; Kukkadapu, R. K.; Zeng, Q.; Edelmann, R. E.; Pentrák, M.; Agrawal, A. Biological redox cycling of iron in nontronite and its potential application in nitrate removal. *Environ. Sci. Technol.* **2015**, *49* (9), 5493−5501.

(19) Christiansen, B. C.; Geckeis, H.; Marquardt, C. M.; Bauer, A.; Romer, J.; Wiss, T.; Schild, D.; Stipp, S. L. S. Neptunyl (NpO_2^+) interaction with green rust, GR(Na,SO_4). *Geochim. Cosmochim. Acta* **2011**, *75* (5), 1216−1226.

(20) Marsac, R.; Banik, N. L.; Lutzenkirchen, J.; Marquardt, C. M.; Dardenne, K.; Schild, D.; Rothe, J.; Diascorn, A.; Kupcik, T.; Schafer, T.; Geckeis, H. Neptunium redox speciation at the Illite surface. *Geochim. Cosmochim. Acta* **2015**, *152*, 39−51.

(21) Yang, J.; Kukkadapu, R. K.; Dong, H.; Shelobolina, E. S.; Zhang, J.; Kim, J. Effects of redox cycling of iron in nontronite on reduction of technetium. *Chem. Geol.* **2012**, *291*, 206−216.

(22) Law, G. T. W.; Geissler, A.; Burke, I. T.; Livens, F. R.; Lloyd, J. R.; McBeth, J. M.; Morris, K. Uranium redox cycling in sediment and biomineral systems. *Geomicrobiol. J.* **2011**, *28* (5−6), 497−506.

DOI: 10.1021/acs.est.5b03463
Environ. Sci. Technol. 2015, 49, 13139−13148

(23) Begg, J. D. C.; Burke, I. T.; Lloyd, J. R.; Boothman, C.; Shaw, S.; Charnock, J. M.; Morris, K. Bioreduction behavior of U(VI) sorbed to sediments. *Geomicrobiol. J.* **2011**, *28* (2), 160−171.
(24) Campbell, K. M.; Kukkadapu, R. K.; Qafoku, N. P.; Peacock, A. D.; Lesher, E.; Williams, K. H.; Bargar, J. R.; Wilkins, M. J.; Figueroa, L.; Ranville, J.; Davis, J. A.; Long, P. E. Geochemical, mineralogical and microbiological characteristics of sediment from a naturally reduced zone in a uranium-contaminated aquifer. *Appl. Geochem.* **2012**, *27* (8), 1499−1511.
(25) Zhang, G. X.; Burgos, W. D.; Senko, J. M.; Bishop, M. E.; Dong, H. L.; Boyanov, M. I.; Kemner, K. M. Microbial reduction of chlorite and uranium followed by air oxidation. *Chem. Geol.* **2011**, *283* (3−4), 242−250.
(26) Lee, J. H.; et al. Microbial reductive transformation of phyllosilicate Fe(III) and U(VI) in fluvial subsurface sediments. *Environ. Sci. Technol.* **2012**, *46* (7), 3721−3730.
(27) Latta, D. E.; Gorski, C. A.; Boyanov, M. I.; O'Loughlin, E. J.; Kemner, K. M.; Scherer, M. M. Influence of magnetite stoichiometry on U-VI reduction. *Environ. Sci. Technol.* **2012**, *46* (2), 778−786.
(28) Veeramani, H.; Alessi, D. S.; Suvorova, E. I.; Lezama-Pacheco, J. S.; Stubbs, J. E.; Sharp, J. O.; Dippon, U.; Kappler, A.; Bargar, J. R.; Bernier-Latmani, R. Products of abiotic U(VI) reduction by biogenic magnetite and vivianite. *Geochim. Cosmochim. Acta* **2011**, *75* (9), 2512−2528.
(29) Ilton, E. S.; Heald, S. M.; Smith, S. C.; Elbert, D.; Liu, C. X. Reduction of uranyl in the interlayer region of low iron micas under anoxic and aerobic conditions. *Environ. Sci. Technol.* **2006**, *40* (16), 5003−5009.
(30) Boyanov, M. I.; O'Loughlin, E. J.; Roden, E. E.; Fein, J. B.; Kemner, K. M. Adsorption of Fe(II) and U(VI) to carboxyl-functionalized microspheres: the influence of speciation on uranyl reduction studied by titration and XAFS. *Geochim. Cosmochim. Acta* **2007**, *71* (8), 1898−1912.
(31) Singer, D. M.; Maher, K.; Brown, G. E. Uranyl-chlorite sorption/desorption: evaluation of different U(VI) sequestration processes. *Geochim. Cosmochim. Acta* **2009**, *73* (20), 5989−6007.
(32) Ilton, E. S.; Haiduc, A.; Moses, C. O.; Heald, S. M.; Elbert, D. C.; Veblen, D. R. Heterogeneous reduction of uranyl by micas: crystal chemical and solution controls. *Geochim. Cosmochim. Acta* **2004**, *68* (11), 2417−2435.
(33) Cutting, R. S.; Coker, V. S.; Telling, N. D.; Kimber, R. L.; Pearce, C. I.; Ellis, B. L.; Lawson, R. S.; Van der Laan, G.; Pattrick, R. A. D.; Vaughan, D. J.; Arenholz, E.; Lloyd, J. R. Optimizing Cr(VI) and Tc(VII) remediation through nanoscale biomineral engineering. *Environ. Sci. Technol.* **2010**, *44* (7), 2577−2584.
(34) Lovley, D. R.; Phillips, E. J. P. Rapid assay for microbially reducible ferric iron in aquatic sediments. *Appl. Environ. Microbiol.* **1987**, *53* (7), 1536−1540.
(35) von Canstein, H.; Ogawa, J.; Shimizu, S.; Lloyd, J. R. Secretion of flavins by Shewanella species and their role in extracellular electron transfer. *Appl. Environ. Microbiol.* **2008**, *74* (3), 615−23.
(36) Johnson, D. A.; Florence, T. M. Spectrophotometric determination of uranium(VI) with 2-(5-Bromo-2- pyridylazo)-5-diethylaminophenol. *Anal. Chim. Acta* **1971**, *53* (1), 73−79.
(37) Hess, N. J.; Xia, Y. X.; Rai, D.; Conradson, S. D. Thermodynamic model for the solubility of $TcO_2 \bullet xH_2O$ (am) in the aqueous Tc(IV)-Na^+-Cl^--H^+-OH^--H_2O system. *J. Solution Chem.* **2004**, *33* (2), 199−226.
(38) Scheinost, A. C.; Schmeisser, N.; Banerjee, D.; Rossberg, A.; Denecke, M.; Dardenne, K.; Rothe, J.; Daehn, R. Ac XAS an actinide reference X-ray absorption spectroscopy database. 2013. https://www.hzdr.de/acxas (accessed Oct 1, 2015).
(39) Hennig, C.; Ikeda-Ohno, A.; Tsushima, S.; Scheinost, A. C. The sulfate coordination of Np(IV), Np(V), and Np(VI) in aqueous solution. *Inorg. Chem.* **2009**, *48* (12), 5350−5360.
(40) Dent, A. J.; Cibin, G.; Ramos, S.; Smith, A. D.; Scott, S. M.; Varandas, L.; Pearson, M. R.; Krumpa, N. A.; Jones, C. P.; Robbins, P. E. B18: A core XAS spectroscopy beamline for Diamond. *J. Phys.: Conf. Ser.* **2009**, *190* (1), 012039.
(41) Rothe, J.; Butorin, S.; Dardenne, K.; Denecke, M. A.; Kienzler, B.; Loeble, M.; Metz, V.; Seibert, A.; Steppert, M.; Vitova, T.; Walther, C.; Geckeis, H. The INE-Beamline for actinide science at ANKA. *Rev. Sci. Instrum.* **2012**, *83*, 043105.
(42) Ravel, B.; Newville, M. ATHENA, ARTEMIS, HEPHAESTUS: data analysis for X-ray absorption spectroscopy using IFEFFIT. *J. Synchrotron Radiat.* **2005**, *12*, 537−541.
(43) Ankudinov, A. L.; Ravel, B.; Rehr, J. J.; Conradson, S. D. Real-space multiple-scattering calculation and interpretation of X-ray-absorption near-edge structure. *Phys. Rev. B: Condens. Matter Mater. Phys.* **1998**, *58* (12), 7565−7576.
(44) Brookshaw, D. R.; Lloyd, J. R.; Vaughan, D. J.; Pattrick, R. A. D. Bioreduction of biotite and chlorite by a Shewanella species. *Am. Mineral.* **2014**, *99* (8−9), 1746−1754.
(45) Behrends, T.; Van Cappellen, P. Competition between enzymatic and abiotic reduction of uranium(VI) under iron reducing conditions. *Chem. Geol.* **2005**, *220* (3−4), 315−327.
(46) Waite, T. D.; Davis, J. A.; Payne, T. E.; Waychunas, G. A.; Xu, N. Uranium (VI) adsorption to ferrihydrite - application of a surface complexation model. *Geochim. Cosmochim. Acta* **1994**, *58* (24), 5465−5478.
(47) Belli, K. M.; DiChristina, T. J.; Van Cappellen, P.; Taillefert, M. Effects of aqueous uranyl speciation on the kinetics of microbial uranium reduction. *Geochim. Cosmochim. Acta* **2015**, *157*, 109−124.
(48) Heald, S. M.; Krupka, K. M.; Brown, C. F. Incorporation of pertechnetate and perrhenate into corroded steel surfaces studied by X-ray absorption fine structure spectroscopy. *Radiochim. Acta.* **2012**, *100* (4), 243−253.
(49) Marshall, T. A.; Morris, K.; Law, G. T. W.; Mosselmans, J. F. W.; Bots, P.; Parry, S. A.; Shaw, S. Incorporation and retention of ^{99}Tc(IV) in magnetite under high pH conditions. *Environ. Sci. Technol.* **2014**, *48* (20), 11853−11862.
(50) Zachara, J. M.; Heald, S. M.; Jeon, B.-H.; Kukkadapu, R. K.; Liu, C.; McKinley, J. P.; Dohnalkova, A. C.; Moore, D. A. Reduction of pertechnetate [Tc(VII)] by aqueous Fe(II) and the nature of solid phase redox products. *Geochim. Cosmochim. Acta* **2007**, *71* (9), 2137−2157.
(51) Fredrickson, J. K.; Zachara, J. M.; Plymale, A. E.; Heald, S. M.; McKinley, J. P.; Kennedy, D. W.; Liu, C.; Nachimuthu, P. Oxidative dissolution potential of biogenic and abiogenic TcO_2 in subsurface sediments. *Geochim. Cosmochim. Acta* **2009**, *73* (8), 2299−2313.
(52) Morris, K.; Livens, F.; Charnock, J.; Burke, I.; McBeth, J.; Begg, J.; Boothman, C.; Lloyd, J. An X-ray absorption study of the fate of technetium in reduced and reoxidised sediments and mineral phases. *Appl. Geochem.* **2008**, *23*, 603−617.
(53) Liu, J.; Pearce, C. I.; Qafoku, O.; Arenholz, E.; Heald, S. M.; Rosso, K. M. Tc(VII) reduction kinetics by titanomagnetite nanoparticles. *Geochim. Cosmochim. Acta* **2012**, *92*, 67−81.
(54) Szecsody, J. E.; Jansik, D. P.; McKinley, J. P.; Hess, N. J. Influence of alkaline co-contaminants on technetium mobility in vadose zone sediments. *J. Environ. Radioact.* **2014**, *135*, 147−160.
(55) Docrat, T. I.; Mosselmans, J. F. W.; Charnock, J. M.; Whiteley, M. W.; Collison, D.; Livens, F. R.; Jones, C.; Edmiston, M. J. X-ray absorption spectroscopy of tricarbonatodioxouranate(V), $[UO_2(CO_3)]^{5-}$, in aqueous solution. *Inorg. Chem.* **1999**, *38* (8), 1879−1882.
(56) Rossberg, A.; Ulrich, K.-U.; Weiss, S.; Tsushima, S.; Hiemstra, T.; Scheinost, A. C. Identification of uranyl surface complexes on ferrihydrite: advanced EXAFS data analysis and CD-MUSIC modeling. *Environ. Sci. Technol.* **2009**, *43* (5), 1400−1406.
(57) Conradson, S. D. Local structure and charge distribution in the UO_2-U_4O_9 system. *Inorg. Chem.* **2004**, *43* (22), 6922−6935.
(58) Suzuki, Y.; Kelly, S. D.; Kemner, K. M.; Banfield, J. F. Nanometre-size products of uranium bioreduction. *Nature* **2002**, *419* (6903), 134.
(59) Boyanov, M. I.; Fletcher, K. E.; Kwon, M. J.; Rui, X.; O'Loughlin, E. J.; Löffler, F. E.; Kemner, K. M. Solution and microbial controls on the formation of reduced U(IV) species. *Environ. Sci. Technol.* **2011**, *45* (19), 8336−8344.

DOI: 10.1021/acs.est.5b03463
Environ. Sci. Technol. 2015, 49, 13139−13148

(60) Newsome, L.; Morris, K.; Shaw, S.; Trivedi, D.; Lloyd, J. R. The stability of microbially reduced U(IV); impact of residual electron donor and sediment ageing. *Chem. Geol.* **2015**, *409*, 125−135.
(61) Fuchs, L. H.; Gebert, E. X-ray studies of synthetic coffinite, thorite, and uranothorite. *Am. Mineral.* **1958**, *43*, 243−248.
(62) Dreissig, I.; Weiss, S.; Hennig, C.; Bernhard, G.; Zanker, H. Formation of uranium(IV)-silica colloids at near-neutral pH. *Geochim. Cosmochim. Acta* **2011**, *75* (2), 352−367.
(63) Husar, R.; Hübner, R.; Hennig, C.; Martin, P. M.; Chollet, M.; Weiss, S.; Stumpf, T.; Zänker, H.; Ikeda-Ohno, A. Intrinsic formation of nanocrystalline neptunium dioxide under neutral aqueous conditions relevant to deep geological repositories. *Chem. Commun.* **2015**, *51*, 1301−1304.
(64) Fröhlich, D. R.; Amayri, S.; Drebert, J.; Grolimund, D.; Huth, J.; Kaplan, U.; Krause, J.; Reich, T. Speciation of Np(V) uptake by Opalinus Clay using synchrotron microbeam techniques. *Anal. Bioanal. Chem.* **2012**, *404* (8), 2151−2162.
(65) Neumann, A.; Olson, T. L.; Scherer, M. M. Spectroscopic evidence for Fe(II)-Fe(III) electron transfer at clay mineral edge and basal sites. *Environ. Sci. Technol.* **2013**, *47* (13), 6969−6977.

DOI: 10.1021/acs.est.5b03463
Environ. Sci. Technol. 2015, 49, 13139−13148